Advances in Geo-Energy Research

Vol. 15, No. 1, p. 13-26, 2025

Original article

Secondary cracking characteristics of asphaltenes and insights into the reservoir unblocking during oil shale *in-situ* exploitation

Wei Guo[1,2,3,4], Cunhan Fan[1,2,3,4], Sunhua Deng[1,2,3,4], Haoche Shui[1,2,3,4], Zhao Liu[1,2,3,4]*

[1]*College of Construction Engineering, Jilin University, Changchun 130021, P. R. China*

[2]*National-Local Joint Engineering Laboratory of in Situ Conversion, Drilling and Exploitation Technology for Oil Shale, Jilin University, Changchun 130021, P. R. China*

[3]*Provincial and Ministerial Co-construction of Collaborative Innovation Center for Shale Oil & Gas Exploration and Development, Jilin University, Changchun 130021, P. R. China*

[4]*Key Lab of Ministry of Natural Resources for Drilling and Exploitation Technology in Complex Conditions, Changchun 130021, P. R. China*

Keywords:
Oil shale
asphaltene
secondary cracking
mass loss
reservoir blockage

Cited as:
Guo, W., Fan, C., Deng, S., Shui, H., Liu, Z. Secondary cracking characteristics of asphaltenes and insights into the reservoir unblocking during oil shale *in-situ* exploitation. Advances in Geo-Energy Research, 2025, 15(1): 13-26.
https://doi.org/10.46690/ager.2025.01.03

Abstract:
In-situ conversion is essential for the development of oil shale resources. Reservoir blockage has been confirmed to be a technological bottleneck via laboratory-scale experiments and field tests. This issue arises from the precipitated asphaltene and its thickening effect on the pyrolysis oil. Promoting *in-situ* secondary cracking of asphaltene has the potential to mitigate blockage. However, the secondary cracking characteristics of asphaltene have not yet been determined. In this study, asphaltenes were obtained under different pyrolysis temperatures, atmospheres and duration times, their secondary cracking mechanisms were investigated. These findings demonstrate considerable mass loss and discrepant reaction processes across different asphaltenes. Firstly, the mass loss of asphaltenes exceeds 80% at 500 °C for all the samples, and the released space can restore reservoir permeability. Second, based on the evolution of the activation energies and pyrolysis gas components, the asphaltenes obtained under severe conversion conditions undergo pyrolysis defined by synchronous two-stage reactions, whereas the asphaltenes obtained under mild conversion conditions undergo pyrolysis defined by sequential three-stage reactions. Finally, a method for eliminating reservoir blockage was proposed based on the above theories, involving inhibiting asphaltene migration and promoting its *in-situ* secondary cracking by controlling the parameters of the heat-carrying fluid, thereby achieving an unaffected reservoir or reservoir self-unblocking. The obtained results can provide valuable references for the *in-situ* exploitation of oil shale.

1. Introduction

Oil shale is a mineral resource abundant in organic matter, predominantly kerogen, which can crack to shale oil when heated to ~350 °C (Na et al., 2012; Sun et al., 2019; Kang et al., 2020a). Consequently, oil shale is considered a significant complement and alternative to crude oil (Metz, 1974; Qian et al., 2003; Han et al., 2014). Given the formidable environmental problems such as harmful residues, exhaust gas, and liquids on the surface, the surface retorting of oil shale has long been controversial. Underground *in-situ* conversion exploitation is

Yandy Scientific Press

*Corresponding author.
E-mail address: guowei6981@jlu.edu.cn (W. Guo); fanch22@mails.jlu.edu.cn (C. Fan); denghua13@163.com (S. Deng); shuihc21@mails.jlu.edu.cn (H. Shui); zhaoliu@jlu.edu.cn (Z. Liu).

Received August 14, 2024; revised September 25, 2024; accepted October 24, 2024; available online November 2, 2024.

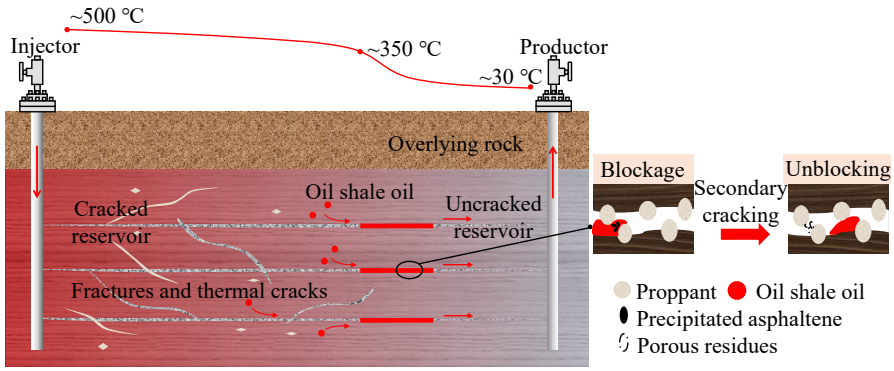

Fig. 1. Diagram of the oil shale reservoir blockage and unblocking due to the asphaltene behavior.

recognized as a highly promising method for the utilization of oil shales. This technique involves artificially heating the in-situ oil shale by injecting a heat-carrying fluid, and the injected heat induces kerogen conversion into oil and gas, followed by oil extraction (Brandt, 2008; He et al., 2021; Pan et al., 2023). This method has potential for the development of deep oil shale, given its small footprint and low environmental impact.

Researchers have extensively investigated the pyrolytic transformation of kerogen (Lai et al., 2017; Shi et al., 2017; Qing et al., 2022), product composition (Yan et al., 2009; Kumar et al., 2013; Xu et al., 2021), and *in-situ* exploitation technologies (Pei et al., 2018; Kang et al., 2020a; Hu et al., 2022). The mechanism and energy consumption of the conversion of solid kerogen into oil and gas were investigated. In addition, established *in-situ* exploitation technologies for oil shale, such as Shell *in-situ* conversion process (Brandt, 2008; Allix et al., 2010), *in-situ* steam injection technology from Taiyuan University of Technology (Wang et al., 2019; Kang et al., 2020a, 2020b), and autothermic pyrolysis *in-situ* conversion process from Jilin University (Guo et al., 2022, 2023), have been well tested. Several of these technologies have been validated through pilot tests. However, relevant studies have highlighted the technical challenges in realizing the industrial application of these technologies. One of the key technical issues is the precipitated asphaltene and its thickening effect on pyrolysis oil, which impairs the reservoir permeability because the concentration of asphaltene in the shale oil is notably high, reaching approximately 30% under low-temperature conditions (Kang et al., 2022) with a pronounced polarity (Fei et al., 2012; Wu et al., 2016; Luo et al., 2024), intensifying the impact of asphaltene behavior on reservoir permeability. Such issues have been frequently encountered in both laboratory experiments and field tests. For instance, core-scale experiments conducted by Martins et al. (2010) demonstrated that the blockage of fluid channels by heavy oil significantly affects core permeability and oil recovery. Previous high-temperature and high-pressure experiments have shown that the fluid injection pressure doubles after the production of pyrolysis oil, which is speculated to be due to a blockage caused by heavy oil (Guo et al., 2022). A similar phenomenon was also observed during *in-situ* pyrolysis pilot tests of oil shale in the Songliao Basin, China, leading to an almost complete halt of oil shale *in-situ* pyrolysis (Liu et al., 2020). The secondary cracking of asphaltene occurs with the increase in reservoir temperature, and the conversion from the asphaltene to porous residues may exhibit a self-unblocking effect, offering insights into restoring the permeability of the reservoir (Fig. 1). Therefore, it is imperative to understand the secondary cracking characteristics of asphaltene to mitigate reservoir blockages during *in-situ* exploitation.

However, most existing studies have focused on the secondary cracking of asphaltenes obtained from different crude oil samples (Akmaz et al., 2012; Tirado et al., 2023), with limited attention given to asphaltenes in shale oil. Furthermore, none of the current oil shale cracking reaction models consider the pyrolysis of asphaltene. For instance, Khulbe et al., 1984 investigated the cracking process of asphaltene in the Cold Lake region in Canada using thermogravimetric (TG) analysis. They observed that a significant portion of the asphaltene was converted into oil during hydrotreatment. Similarly, Douda et al. (2008) and Saitova et al. (2021) analyzed the cracking of asphaltenes in different crude oils and the changes in asphaltene in Maya crude oil during pyrolysis. They obtained the components of the pyrolysis products of asphaltene in Maya crude oil and revealed that asphaltene in vacuum residual oil underwent a single pyrolysis stage. Different atmospheres and methods have also been adopted to investigate the thermal cracking of asphaltenes. For example, Pei et al. (2020) compared the cracking reactions of asphaltene from the Liaohe Oilfield in China under various atmospheres and found that the presence of air had a negative effect on the cracking of oil products. Rüger et al. (2022) used a thermal-optical carbon analyzer combined with a high-resolution mass spectrometer to study the thermal cracking behavior of asphaltenes in a variety of crude oils. Liu et al. (2021) studied the formation of light aromatic hydrocarbons via the catalytic cracking of coal tar asphaltene using a transition metal ion-modified zeolite. In summary, few relevant studies have been conducted on asphaltene in oil shales, and its cracking mechanisms remain unclear. In addition, several oil shale cracking reactions such as the Braun-Burnham and Wellington models have been developed to describe the oil generation process based on the cracking mechanisms of liquid oil and kerogen (Braun and Rothman, 1975, 1990; Khakimova et al., 2019). However, these models do not account for asphaltenes; thus, it is difficult to accurately predict the *in situ* exploitation process of oil

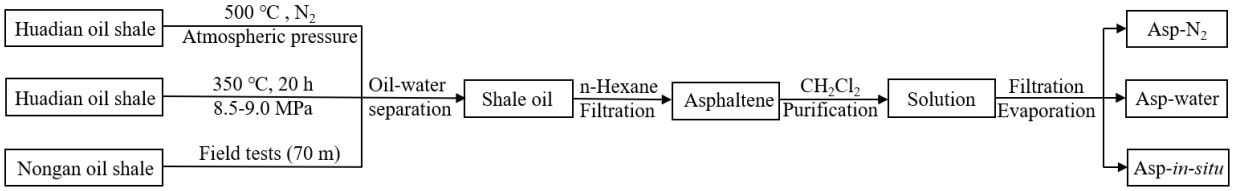

Fig. 2. Preparation process of asphaltenes from oil shale.

shale.

Existing studies are based on isolated asphaltene in crude oil, which is formed by natural hydrocarbon generation over a long period. However, the asphaltene in shale oil is the product of rapid cracking of solid kerogen at a temperature above 350 °C, and it has undergone the initial cracking. Therefore, the secondary cracking characteristics of the two samples were not identical. Studies on the secondary cracking of asphaltene in shale oil not only provide a reference for establishing a comprehensive oil shale cracking reaction model but also provide a theoretical basis for eliminating reservoir blockage. In this study, different asphaltene samples were extracted through oil shale pyrolysis, and their secondary cracking characteristics were determined by TG analysis. Combined with the changes in the pyrolysis products determined by Fourier transform infrared spectroscopy (FTIR) and reaction kinetics analyses, the cracking mechanisms of the asphaltenes were determined. Finally, insights into regulating the separation of oil multi-components during oil shale *in-situ* exploitation are given, and a method for eliminating reservoir blockage is proposed. These findings can guide efforts to control reservoir permeability and enhance the quality of produced oil.

2. Materials and methods

2.1 Sample preparation

The asphaltene content, structure, and properties of the shale oil obtained using different production processes were significantly different. To obtain a reference for migrating reservoir blockages encountered in various *in-situ* exploitation processes, the secondary cracking of asphaltenes in different shale oils must be investigated comprehensively. Therefore, three asphaltene samples were prepared for experimentation:

1) Asphaltenes referred to as asphaltenes-N_2 (Asp-N_2) were obtained by conducting oil shale pyrolysis at 500 °C in a nitrogen atmosphere at atmospheric pressure, followed by the separation of asphaltenes from the shale oil, corresponding to high-temperature fluid convection heating process;
2) Asphaltenes referred to as asphaltenes-water (Asp-water) were acquired by subjecting shale oil to pyrolysis under low temperature and high pressure conditions with water at 350 °C for an extended duration. This sample was chosen because the asphaltene content in pyrolysis oil exceeded 30% under these conditions.
3) Asphaltenes referred to as asphaltenes-*in-situ* (Asp-*in-situ*) were separated from shale oil produced during the underground *in-situ* pyrolysis field test in the Songliao Basin of China.

Oil shale samples from the Huadian and Nongan regions of the Songliao Basin were used to enhance the applicability of the results of this study. Asphaltene undergoes varying degrees of cracking during the preparation of shale oil; therefore, the reaction of asphaltene in the TG experiments was defined as secondary cracking. The asphaltene preparation process is illustrated in Fig. 2. The preparation and purification processes are described in detail as follows.

2.1.1 Preparation of shale oil samples

Preparation of shale oil for isolating Asp-N_2 samples: Oil shale samples from the Huadian area of the Songliao Basin, China, were selected as the research objects. A total of 40 g oil shale particles (diameter 0.4-1.7 mm) were dried in an oven at 80 °C for 12 h, and then placed in a quartz distillation apparatus (inner diameter 50 mm; height 140 mm). The oil shale was heated from 30-500 °C at a heating rate of 10 °C/min under N_2 purge gas and held for 2 h. The N_2 flow rate was 40 ml/min to quickly remove the oil and gas products generated by oil shale cracking and simulate rapid pyrolysis by heating oil shale with high-temperature fluid convection. High-temperature products were collected using a low-temperature water-cooling device.

Preparation method of shale oil for isolating Asp-water samples: Huadian oil shale samples (150 g) under the same parameters were placed in a 0.5 L high-temperature and high-pressure reactor and filled with 300 ml of distilled water to simulate a stratigraphic water environment; then, the reactor was sealed. The reactor vessel was heated to 350 °C, maintaining a pressure of 8.5-9.0 MPa, and the reaction was sustained for 20 h to simulate low-temperature long-term pyrolysis. The oil products were collected after the reactor cooled to room temperature.

Preparation method of shale oil for isolating Asp-*in-situ* samples: We conducted a field pilot test project in the Songliao Basin, China, with a mining depth of 70 m and well spacing of 5 m (Zhu et al., 2022). Shale oil from the production wells was collected and separated to obtain the Asp-*in-situ* samples.

2.1.2 Separation and purification of asphaltenes

The separation and purification of asphaltene from shale oil adhered to standard NB/SH/T0509-2010. The specific procedure is summarized as follows. First, the shale oil sample obtained from Section 2.1.1 was dissolved in n-heptane. The precipitate obtained after filtration represents the raw asphaltene material. Subsequently, the Soxhlet extraction method was employed to reflux n-heptane with asphaltene at a ratio

of 40:1 (v/w), completely eliminating soluble components in the asphaltene structure. Subsequently, CH_2Cl_2 was utilized to fully reflux and dissolve asphaltene at a ratio of 30:1 (v/w), effectively removing solid impurities such as clay mineral precipitation (Hao et al., 2017). Pure asphaltene samples were obtained by drying.

2.2 Thermogravimetry-Fourier transform infrared spectroscopy (TG-FTIR) analysis

The main products of asphaltene cracking are gases, such as CH_4 and CO_2. Therefore, TG-FTIR was used to describe the evolution of the products. The samples of Asp-N_2, Asp-water, and Asp-*in-situ* were subjected to TG-FTIR analysis using an STA 499 F3 TG analyzer and Nicolet iS10 Fourier transform infrared spectrometer to investigate the thermal decomposition behavior of asphaltenes and obtain information on the gas composition and functional groups generated during pyrolysis. The three samples were sequentially placed in different ceramic crucibles and heated in a nitrogen atmosphere from 20-800 °C at heating rates of 2, 5, and 10 °C min^{-1}. During the experiment, the flow rate of high-quality nitrogen (99.99%) atmosphere was 60 mL min^{-1}, and the sample mass was 10 mg. Each sample was analyzed at least three times to ensure accuracy of the results. The asphaltene samples and pyrolysis residues were then analyzed according to magnified observation using electron microscopy (EM) and field-emission scanning electron microscopy (FESEM).

The pyrolysis gas products were transferred to an FTIR spectrometer through a 1 m long polytetrafluoroethylene tube, which was heated and kept at a constant temperature of 200 °C to avoid condensation of the pyrolytic gas products. The scanned wavenumber range was 400 to 4,000 cm^{-1}, with six scans performed at a resolution of 8 cm^{-1}.

2.3 Infrared pressing experiment

A Nicolet iS10 Fourier transform infrared spectrometer was used to detect the asphaltene and pyrolysis residue using FTIR compression films to obtain the material composition and functional group information before and after the pyrolysis of asphaltene.

First, the spectral-grade potassium bromide sample purchased from Aladdin (USA) was ground in a mortar for approximately 3 min until it reached a flour-like state; then, the potassium bromide sample was placed in a film mold and pressed to 10^{-15} MPa for 5 min. Baseline information was obtained by infrared detection of transparent potassium bromide tablets. Subsequently, the three types of asphaltenes were used to prepare a mixture of potassium bromide and asphaltene in a ratio of approximately 100:1 for infrared detection. Each set of asphaltenes was tested thrice to ensure the accuracy of the experimental data.

2.4 Reaction kinetics analysis

2.4.1 Gaussian multi-peak fitting

Gaussian multipeak fitting is a widely accepted method for analyzing multiple reactions and is achieved by separating and analyzing overlapping peaks in asymmetric curves through numerical calculations and mathematical methods (Ma et al., 2008; Li et al., 2010). In this study, Gaussian multi-peak fitting was used to fit the curves of the transformation rates of different asphaltenes and qualitatively divide the reaction stages combined with the changes in activation energy (Ma et al., 2024). R^2 reflects the degree of fit of the curve. The closer R^2 is to 1, the better the fitting effect. The degree of fit was evaluated using the residual sum of squares (S) and the correlation coefficient, R^2. The smaller the S value, the higher the calculation precision is (Wang et al., 2013).

The expression of the equation for S is (Gregorčič and Lightbody, 2009):

$$S = \sum_{i=1}^{n} \omega_i [y_i - f_i(\chi_i)]^2 \tag{1}$$

where ω_i is the weighted factor, dimensionless; y_i and f_i are experimental data and fitting data in Gaussian multi-peak fitting, $°C^{-1}$; n and i are the number of iterations, dimensionless; and χ is the evaluation function, dimensionless.

2.4.2 Calculation of activation energy

Kinetic models are the primary approach for determining the activation energy of a chemical reaction. This study employed the Friedman, Flynn-Wall-Ozawa (FWO), and Kissinger-Akihiro-Sunose (KAS) kinetic methods to calculate the activation energies of different pyrolysis reactions.

During kinetic analysis, the basic rate equation is expressed as:

$$\frac{d\alpha}{dt} = kf(\alpha) \quad \text{or} \quad \frac{d\alpha}{dT} = \frac{A}{\beta}\exp\left(-\frac{E}{RT}\right)f(\alpha) \tag{2}$$

where α is the conversion rate and represents the reaction degree of the sample, which can be expressed as $\alpha = (m_0 - m_T)/(m_0 - m_\infty)$, dimensionless; k is the reaction rate constant, dimensionless; β is the heating rate, °/min; t is time, min; m_0 is the initial mass of the sample, mg; m_t is the mass of the sample at reaction time t, mg; m_∞ is the final mass of the sample, mg; A refers to the pre-factor, S^{-1}; E is the apparent activation energy, $kJ{\cdot}mol^{-1}$; R is the gas constant, $J{\cdot}mol^{-1}{\cdot}K^{-1}$; T is the reaction temperature, K; and $f(\alpha)$ is the reaction mechanism function that describes the relationship between reaction rate and conversion, dimensionless.

When the heating rate is constant, the heating rate β is defined as follows:

$$\beta = \frac{dT}{dt} \tag{3}$$

in this study, activation energy E was determined using the following three methods:

(1) The Friedman method, which is considered one of the most classical differential iso-conversion methods, is utilized for the direct calculation of the activation energy associated with the primary reaction process, without resorting to approximation. However, its high sensitivity to experimental noise makes it prone to instability in its output value. As follows:

$$\ln\left(\beta\frac{dT}{dt}\right) = \ln A f(\alpha) - \frac{E}{RT} \tag{4}$$

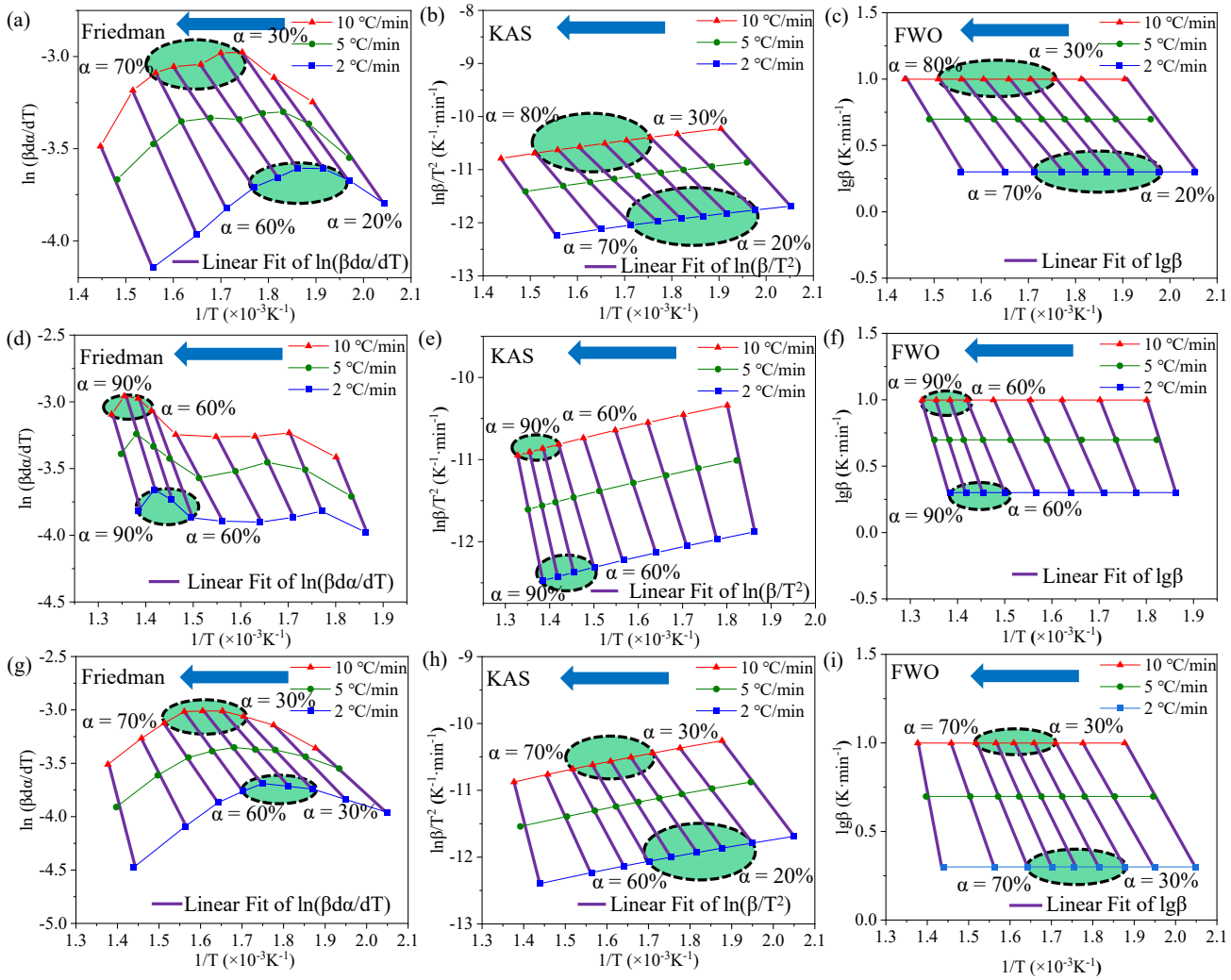

Fig. 3. Arrhenius equation curves for three asphaltenes with various methods. (a)-(c) for Asp-N_2, (d)-(f) for Asp-water, and (g)-(i) for Asp-*in-situ*.

(2) The FWO method is derived from the Doyle approximation for the temperature integral. The error in the method depends on the magnitude of the change in the activation energy relative to the conversion rate. The expressions are as follows:

$$\ln\beta = \ln\frac{AE}{Eg(\alpha)} - 5.331 - 1.052\frac{E}{RT} \tag{5}$$

(3) The KAS method, which uses the Murray and White approximation as the temperature integral, has the following expression:

$$\ln\left(\frac{\beta}{T^2}\right) = \ln\frac{AR}{Eg(\alpha)} - \frac{E}{RT} \tag{6}$$

where $g(\alpha)$ is the integral form of the reaction model:

$$g(\alpha) = \int_0^{\alpha}\frac{\mathrm{d}\alpha}{f(\alpha)} = \frac{A}{\beta}\int_0^{\alpha}\exp\frac{-Ea}{RT}\,\mathrm{d}T \tag{7}$$

At the same conversion rate, $1/T$ is plotted on the X-axis, and $\ln[\beta(\mathrm{d}\alpha/\mathrm{d}t)]$, $\ln\beta$, and $\ln(\beta/T^2)$ are plotted on the Y-axis. Corresponding figures for the Friedman, FWO, and KAS methods were generated. The estimated value of E was derived from the slope of the regression curve fitted to each conversion rate. A graphical representation of the fitting curve is shown in Fig. 3, and the variation in E with conversion rate is illustrated in Fig. 4.

3. Results and discussion

3.1 Thermogravimetric analysis of Asphaltenes

A TG curve is an important means of characterizing the secondary cracking of asphaltene. In this study, TG experiments were conducted on three samples at different heating rates. Fig. 5 shows the mass loss of the three samples at heating rates of 2, 5, and 10 °C/min, stage I to III are divided according to the reaction rates and mass loss, these stages correspond to various pyrolysis peaks which will be explained in the following sections. Across different heating rates, the mass loss curves of each sample exhibited similar shapes as the temperature rose from 30-800 °C. The mass loss of asphaltene was different under various pyrolysis conditions. With an increase in the heating rate, the TG curve

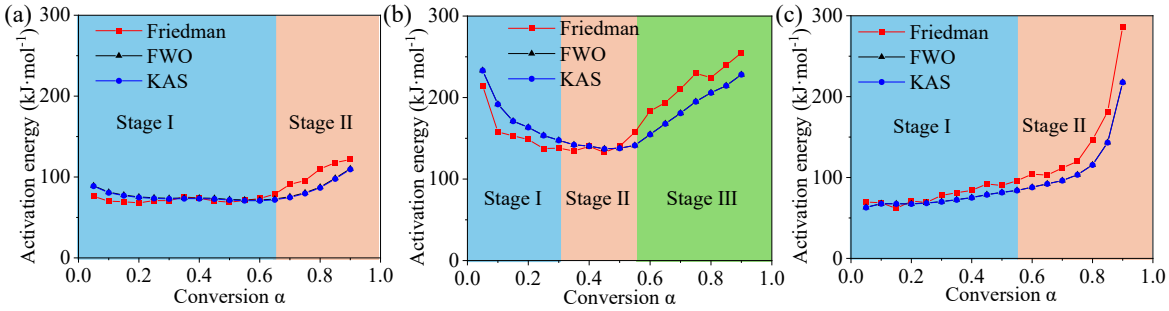

Fig. 4. Activation energy curves of the three asphaltenes during pyrolysis. (a), (b), and (c) represent the samples Asp-N_2, Asp-water, and Asp-*in-situ*, respectively.

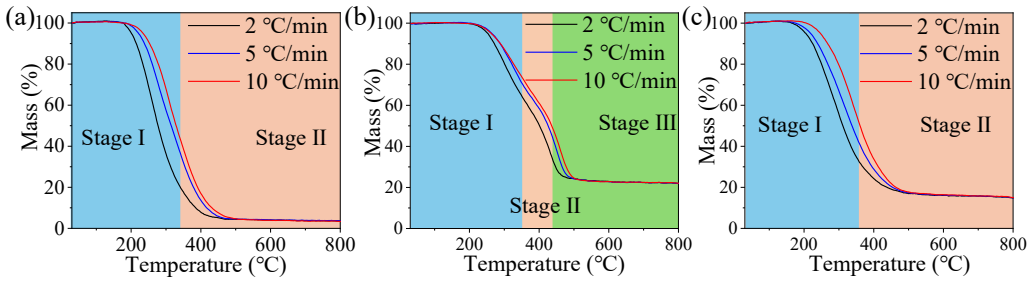

Fig. 5. TG curves of three asphaltenes at different heating rates. (a) TG curves of Asp-N_2 sample, (b) TG curves of Asp-water sample, and (c) TG curves of Asp-*in-situ* sample.

shifted towards higher temperatures. Notably, all three samples reached maximum mass loss at approximately 540 °C. It is also important to highlight that significant variations were observed in the total mass loss among samples, with Asp-N_2 showing a maximum mass loss of approximately 95%; Asp-water exhibiting ~ 80% mass loss, Asp-*in-situ* showing a mass loss of ~ 90%. Thus, asphaltene pyrolysis results in a loss of over 80% of its weight at high temperatures. When asphaltene obstructed the seepage channels in the *in-situ* reservoir owing to its deposition or thickening effect on the pyrolysis oil, the mass loss of asphaltene gradually released its occupied pores as the temperature increased, presenting a self-unblocking effect.

To analyze the differences in the cracking of different asphaltenes, the TG and DTG profiles of the three samples are further compared under a heating rate of 10 °C/min, as illustrated in Fig. 6. Table 1 lists the primary parameters of asphaltene cracking reactions. The mass loss of the three samples primarily occurred within the temperature range of 150-540 °C, with the initial TG temperature falling between 150 and 200 °C, slightly lower than the initial temperature of asphaltenes in crude oil (Murugan et al., 2009; Luo et al., 2024). Initially, the thermal mass loss of asphaltenes was primarily attributed to the evaporation of light hydrocarbon molecules confined within the intricate structure of asphaltene, similar to the physical mass loss phenomenon. Because of the higher abundance of heteroatoms and heightened polarity of asphaltenes in shale oil, asphaltenes adsorb more volatile materials, thereby lowering the initial mass-loss temperatures.

As the temperature gradually increases, distinct mass loss peaks are observed in all three samples at approximately 360 °C. Additionally, the Asp-water sample exhibits a noticeable mass loss peak at 462.7 °C. Previous research has indicated that asphaltene pyrolysis typically exhibited a single mass loss peak around 430 °C. In air, asphaltene pyrolysis reveals two prominent mass loss peaks (Murugan et al., 2009). The above results show that the pyrolysis reaction stage, the pyrolysis starting temperature, and mass loss of asphaltene in shale oil is very different from that in crude oil, and the pyrolysis of the three samples selected in this study is also significantly different. The reaction processes are explained in combination with the activation energies and products.

3.2 Reaction kinetics of secondary cracking

3.2.1 Gaussian multi-peak fitting

As mentioned above, the three samples exhibited different mass-loss peaks, reflecting the various reaction stages of asphaltene cracking. In this study, Gaussian multi-peak fitting was used to fit the curves of conversion rate for the three asphaltenes with a heating rate of 10 °C /min from 150-540 °C; then, the reaction stages of asphaltene cracking were qualitatively divided. As shown in Fig. 7, for Asp-N_2 and Asp-*in-situ*, there is a significant deviation between the calculated value of the Gaussian single-peak fitting and the experimental values. Over the entire temperature range, the Gaussian bi-peak fitting effect was better, with R^2 values of 0.9990 and 0.9984, respectively. This is because the single-peak fitting approximates the secondary cracking of asphaltenes as a single reaction. However, asphaltene is an extremely complex high-molecular-weight organic matter (Vyazovkin et al., 2011; Saitova et al., 2021) that contains a variety of chemical

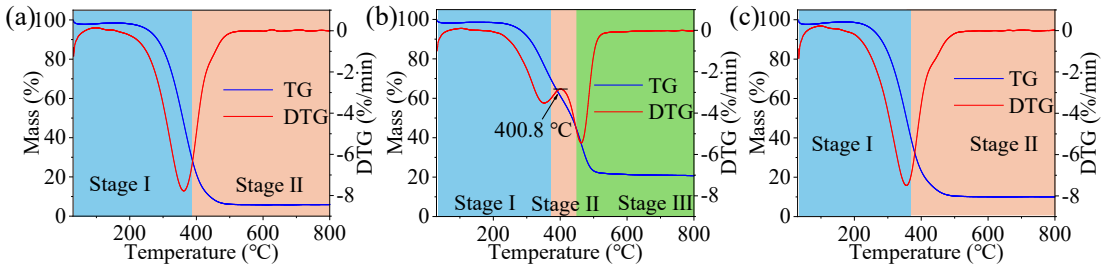

Fig. 6. TG and DTG curves of three asphaltenes at a heating rate of 10 °C/min. (a) Asp-N_2 sample, (b) Asp-water sample, and (c) Asp-*in-situ* sample.

Table 1. Ultimate analysis of asphaltenes.

Sample	Main cracking stage			T_m (°C)		$(dw/dt)_{max}$ (%·min^{-1})		Mass loss (%)
	T_i (°C)	T_t (°C)	$T_t - T_i$ (°C)	T_{m1}	T_{m2}	$(dw/dt)_{max\,1}$	$(dw/dt)_{max\,2}$	
Asp-N_2	153.5	536.3	382.8	362.3	/	-7.76	/	93.8
Asp-water	182.3	536.3	353.7	352	462.7	-3.51	-5.42	79.2
Asp-*in-situ*	150	518	368	355.5	/	-7.5	/	89.6

Notes: T_i represents the pyrolysis start temperature, °C; T_t represents the pyrolysis end temperature, °C; T_{mn} represents the temperature corresponding to the n-th greatest mass loss rate, °C; and $(dw/dt)_{max\,n}$ represents the corresponding rate value for the n-th greatest mass loss rate, $n = 1, 2$.

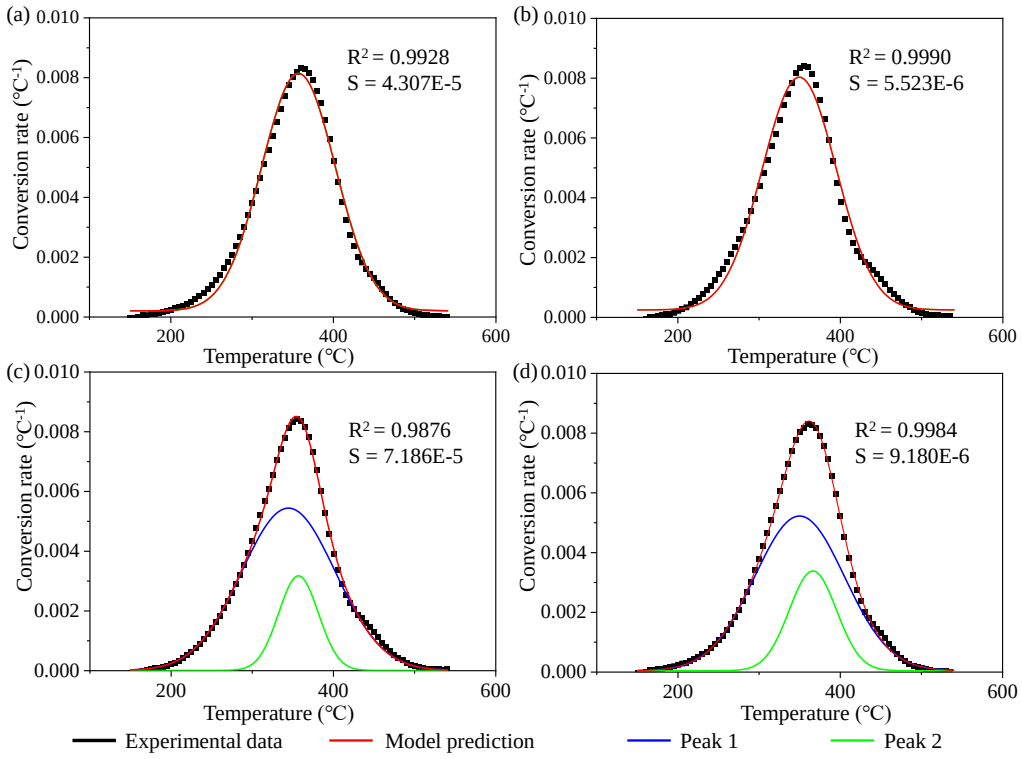

Fig. 7. Gaussian of samples Asp-N_2 and Asp-*in-situ* at a heating rate of 10 °C/min. (a) and (b) are the single-peak and bi-peak fitting of Asp-N_2 sample, respectively, (c) and (d) are the single-peak and bi-peak fitting of Asp-*in-situ* sample, respectively.

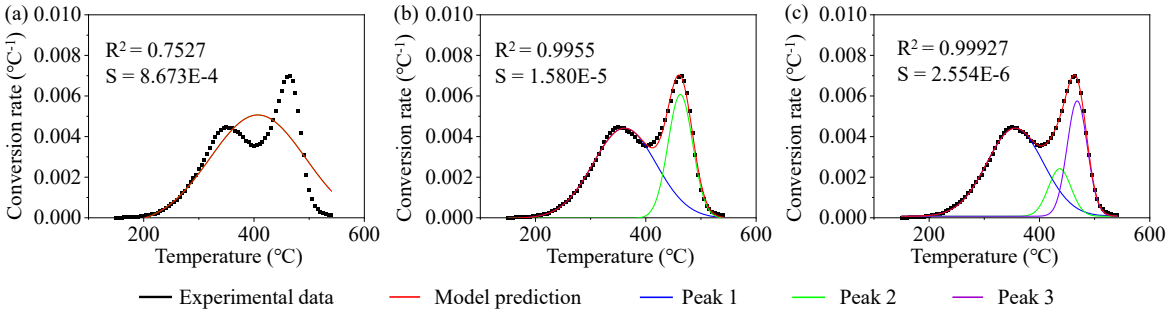

Fig. 8. Gaussian fitting of sample Asp-water at a heating rate of 10 °C/min. (a), (b) and (c) are the single-peak, bi-peak, and three-peak fitting of Asp-water sample, respectively.

bonds, and the breakage of bonds with different energies appears in sequence with an increase in temperature. The Gaussian bi-peak fitting can be explained using a two-stage chemical reaction. As illustrated in Figs. 7(b) and 7(d), the pyrolysis processes of the two asphaltene samples exhibit similarities, encompassing a synchronous two-stage reaction process with matching peak positions and varying intensities, and the temperature of characteristic peak of mass loss reaches approximately 350 °C. In addition, the temperature range of peak 1 spans a wider range (200-500 °C), corresponding to a maximum conversion rate of approximately 0.005 $°C^{-1}$. In contrast, peak 2 occurs within the temperature range of 300-450 °C, with a maximum conversion rate of approximately 0.003 $°C^{-1}$. The initial reaction temperature of peak 1 was relatively low, primarily involving light component evaporation and the primary breakage of chemical bonds with low energy, such as the detachment of side-chain methyl and ethyl groups. In addition, this stage is accompanied by a minor degree of breakage of high-energy bonds. The initial reaction temperature of peak 2 is ∼ 300 °C, and it is presumed to be the initial breakage of bonds with high energy. At this temperature, the breakage of bonds with various energy synchronizations occurs, such as side-chain detachment and breakage of cyclic hydrocarbon rings and chemical bonds containing heteroatoms.

The pyrolysis process of the Asp-water sample was distinctly different. This study utilized Gaussian single-peak, bi-peak, and multi-peak fitting, as shown in Fig. 8. Transitioning from Gaussian single-peak fitting to Gaussian bi-peak fitting, the R^2 value increased from 0.7527 to 0.9955, resulting in significant enhancements in the fitting quality during the initial and final reaction periods, which persisted during the mid-reaction period (Fig. 8(b)). By employing the three-peak fitting approach, although the increment in R^2 was marginal, the overall fitting quality improved substantially, particularly in the middle stage of the reaction. Consequently, the secondary cracking of Asp-water can be categorized as a sequential three-stage reaction process, in which the temperatures of the three peaks increase sequentially. As illustrated in Fig. 8(c), the temperature span of peak 1 ranges between 200-500 °C, aligned with the other two samples; however, the conversion rate diminishes to 0.004 $°C^{-1}$.

The initial temperatures of peak 2 and peak 3 are 380 and 420 °C, respectively. The sequential three-stage reaction process is speculated to occur as follows: Asp-water is subjected to an extended period of low temperature during the preparation of shale oil samples, leading to the depletion of a significant number of chemical bonds with low energies, such as side chains in asphaltene. In the TG experiment, the primary cracking reactions involved the breakage of bonds at high energies, resulting in the regeneration of new side chains. Subsequently, a cracking reaction involving the fracture of low-energy bonds occurs. Finally, at higher temperatures, the breakage of high-energy bonds occurred again. A qualitative description of the asphaltene reaction process was validated through subsequent calculations of the activation energies.

The bond breakage at high energies overlaps with that at low energies. This indicates that the reaction mechanism of the blended components comprises reactions from individual subpeaks (Aboyade et al., 2012). Although increasing the parameter *i* (fitting peak) in the Gaussian fitting may enhance the curve-fitting performance, higher values of *i* do not lead to a significant enhancement in the fitting quality. Moreover, there is a risk of overfitting, irrespective of the increased number of iterations (Nguimbi et al., 2016).

3.2.2 Activation energy of secondary cracking

This section further validates the hypothesis of the asphaltene cracking process in terms of activation energy. The Arrhenius equation plots obtained using different dynamic methodologies are shown in Fig. 3. The observed pyrolysis behavior of distinct asphaltenes is as follows: With increasing heating rates, the locus of the pyrolysis reactions transitions from lower to higher temperature zones and becomes more concentrated. At the same conversion rate, the temperature corresponding to a high heating rate was higher. This implies that the thermal inertia attributable to rapid heating induces the primary reaction to shift towards elevated temperature ranges, consequently diminishing the pyrolysis reactivity of the specimen. Table 2 shows the linear regression coefficients (R^2) derived from the three kinetic approaches, all of which exceed the threshold of 0.98, indicating that the three kinetic methods can better fit the kinetic results.

The activation energies obtained from the calculations during asphaltene pyrolysis are shown in Fig. 4. As shown in the figure, the calculation results differ because of the different

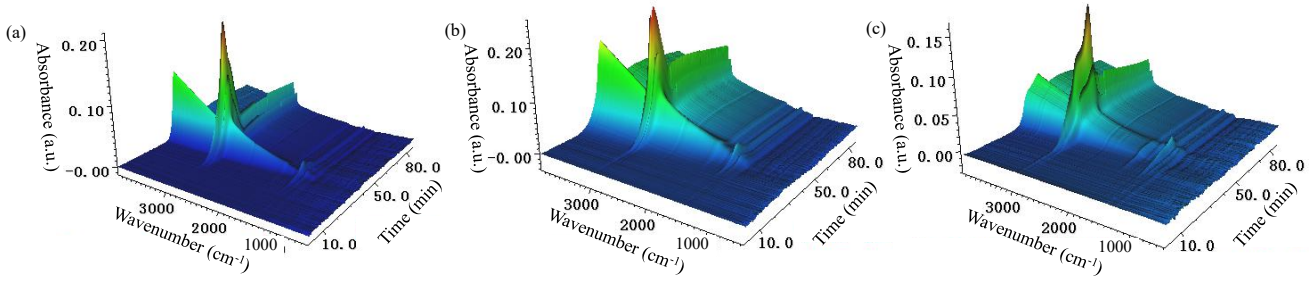

Fig. 9. Three-dimensional TG-FTIR diagrams of pyrolysis gaseous product of three asphaltenes. (a) Asp-N_2, (b) Asp-water, and (c) Asp-*in-situ*.

Table 2. Fit coefficients (R^2) of the linear regression for the three asphaltenes.

	Friedman	FWO	KAS
Asp-N_2	0.99971	0.9929	0.998
Asp-water	0.99944	0.98733	0.99687
Asp-*in-situ*	0.99981	0.9937	0.99377

calculation models. It should be noted that the results obtained by FWO in this study are close to the KAS values. In general, the trend of activation energy E was the same.

By comparing the activation energies of the three samples, the activation energy required for asphaltene cracking in the Asp-N_2 group is found to range between 67 and 120 kJ/mol, with the early stage activation energy stabilizing at a lower value of 70 kJ/mol. When the conversion rate exceeds 0.65, the activation energy gradually increases to approximately 120 kJ/mol. The Asp-*in-situ* sample exhibited a similar trend, yet the final activation energy surpassed 200 kJ/mol. As previously discussed, both the Asp-N_2 and Asp-*in-situ* samples displayed a synchronous two-stage reaction process, and the change in the activation energy indicated that the initial reaction presented low-energy bond breakage. The reaction intensity associated with peak 2 continued to escalate, accompanied by a gradual increase in activation energy, signifying the progression towards bond breakage at low energy. The variation in the activation energy confirmed the hypotheses regarding the pyrolysis mechanism of the two samples.

The secondary cracking of the Asp-water sample was divided into three stages. The minimum activation energy was approximately 140 kJ/mol when the conversion rate was between 0.3 and 0.55, and the activation energies of the early and late stages were higher. The shift in activation energy also verified that the Asp-water sample underwent a sequential three-stage reaction process of high-energy bonds to low-energy bonds, back to high-energy bonds. The Asp-water sample underwent prolonged exposure to low-temperature heat treatment before secondary cracking, thereby leading to a highly polycondensation and aromatized molecular structure. This structural complexity renders the bonds more resistant to breakage, resulting in an overall higher activation energy compared to other asphaltenes and minimal overall mass loss. As the reaction progressed to the later stages, the activation energies of the three samples gradually increased. On the one hand, the fracture of high-energy bonds requires a higher activation energy; on the other hand, at a later stage of the reaction, the inert ash products increased significantly. As a result, pyrolysis of the samples became more difficult, and the apparent activation energy increased (Yang et al., 2022).

3.3 FTIR spectral analysis of gas products

To assess the generation behavior of the pyrolysis gas, the FTIR spectra of the products were analyzed. The three-dimensional TG-FTIR spectra of gaseous byproducts from three different asphaltenes under a heating rate of 10 °C/min are exhibited in Fig. 9. Within the range of 20-55 min (200-550 °C), the spectral vibration peak is notably discernible, signifying the period of asphaltene cracking. By analyzing the three-dimensional FTIR plots in Fig. 9, the infrared spectrum (Fig. 10) can be extracted based on the DTG characteristic temperature points of the asphaltene pyrolysis process, thereby enabling the identification of the constituents within the gas-phase products and their evolution patterns.

Fig. 11 illustrates the evolutionary characteristics of the gas components at various temperatures. Owing to the low activation energy, gas products are produced early with a higher production rate of Asp-N_2 and Asp-*in-situ* asphaltenes, proving that the primary cracking is insufficient, low-energy bonds are abundant, and breakage of these bonds mainly occurs during secondary cracking. During the rapid reaction stage at approximately 350 °C (peak in Figs. 7(b) and 7(d)), the gas production rate experienced a significant surge within the context of the synchronous two-stage reaction process. Subsequently, in the second reaction stage following 400 °C, the pyrolysis reaction progressed towards completion, leading to a gradual decrease in the gas production rate. In contrast, the initial cracking of the Asp-water sample was characterized by high-energy bond, such as in the ring-opening process, resulting in limited gas-phase products. Consequently, the initial temperature of gas production is ∼ 360 °C, corresponding to the initial temperature of the second stage in Fig. 8(c). The peak rate of gas production occurs when the temperature of peak 2 reaches 450 °C, albeit with minimal gas yield when compared to other samples. Subsequently, the gas production rate gradually decreased during the third stage. This phenomenon proves that Asp-water asphaltene undergoes a sequential three-stage reaction process involving

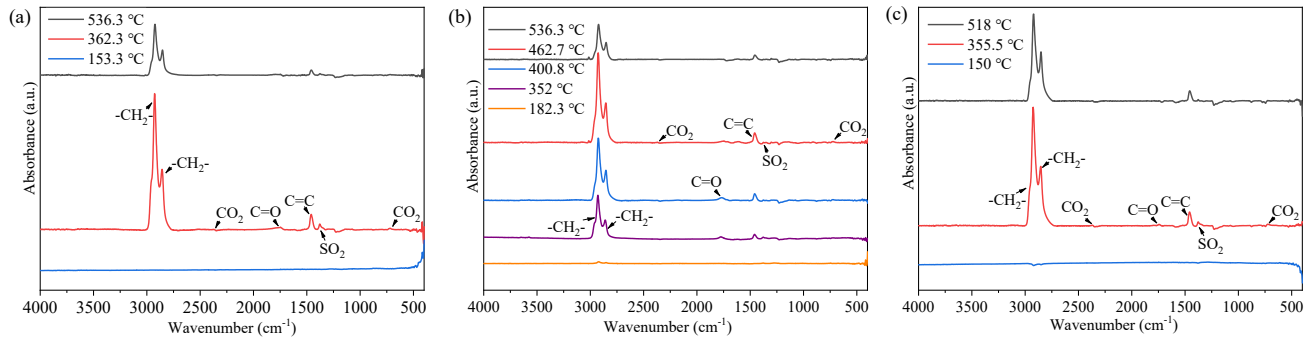

Fig. 10. FTIR spectra of three asphaltenes at different pyrolysis temperatures: (a) Asp-N_2, (b) Asp-water, and (c) Asp-*in-situ*.

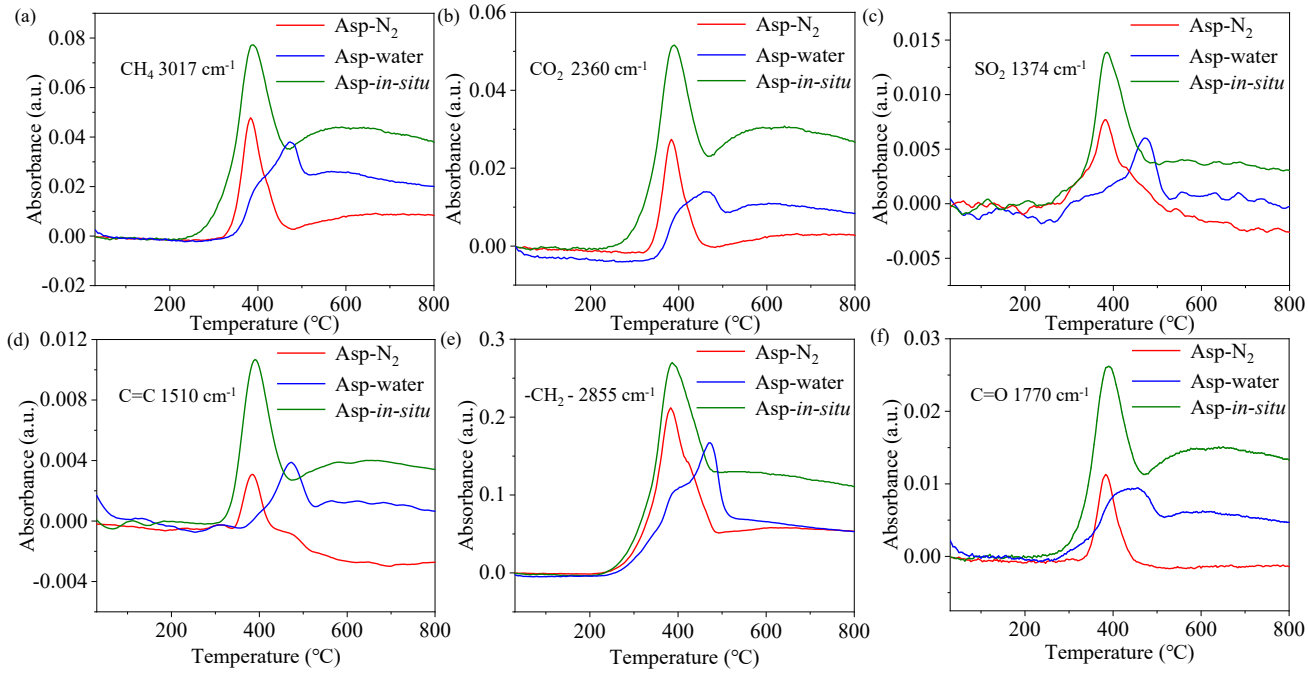

Fig. 11. Evolutionary characteristics of gas products with increasing temperature. (a)-(c) represent the various gas products, (d)-(f) represent the different types of bonds.

high-energy bonds, low-energy bonds, and high-energy bonds at high temperatures.

3.4 Analysis of FTIR compression films

The original forms of the three asphaltenes and pyrolysis residues were compared and analyzed using FTIR compression films. The spectra of the main components of the three samples are shown in Fig. 12. The predominant substances in the original asphaltene were $-CH_2-$ and C=C, which constituted the primary framework of the organic material. The amplitude of the infrared curve indicates the relative content of these components. C=C, which is a low-energy bond susceptible to breakage, exhibited the highest concentration in the original asphaltene of Asp-N_2 and the lowest yet most stable content in the original asphaltene of Asp-water. This finding is consistent with the Gaussian multi-peak fitting analysis and activation energy calculations described above.

The pyrolysis residue of asphaltene contains a low quantity of $-CH_2-$ and C=C components, likely owing to the inadequate and incomplete cracking of certain heavy components. The small S=O content in the residue, not depicted in the figure, suggests that sulfur is predominantly emitted as a pyrolysis gas following asphaltene pyrolysis rather than being retained in the residue.

In the original FTIR image of asphaltene, the tensile vibration of O–H bonds from 3,500-4,000 cm^{-1} is attributed to the adsorption of water from the surrounding atmosphere during the production of the asphaltene FTIR compression films (Gu et al., 2024).

4. Guidance for engineering practice

The temperature and flow rate of the injected fluid play crucial roles in the *in-situ* exploitation of oil shale, particularly in heating oil shale reservoirs. These parameters dictate the heating rate, degree of kerogen cracking, product composition, product distribution, and migration state. Finally, these factors ultimately influence the overall recovery efficiency and economic returns. Although existing studies have ex-

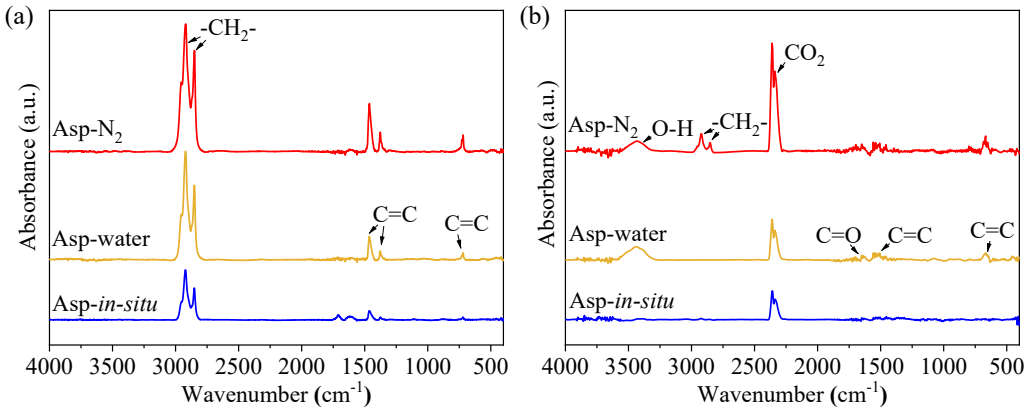

Fig. 12. Infrared results of (a) original asphaltenes and (b) pyrolysis residues.

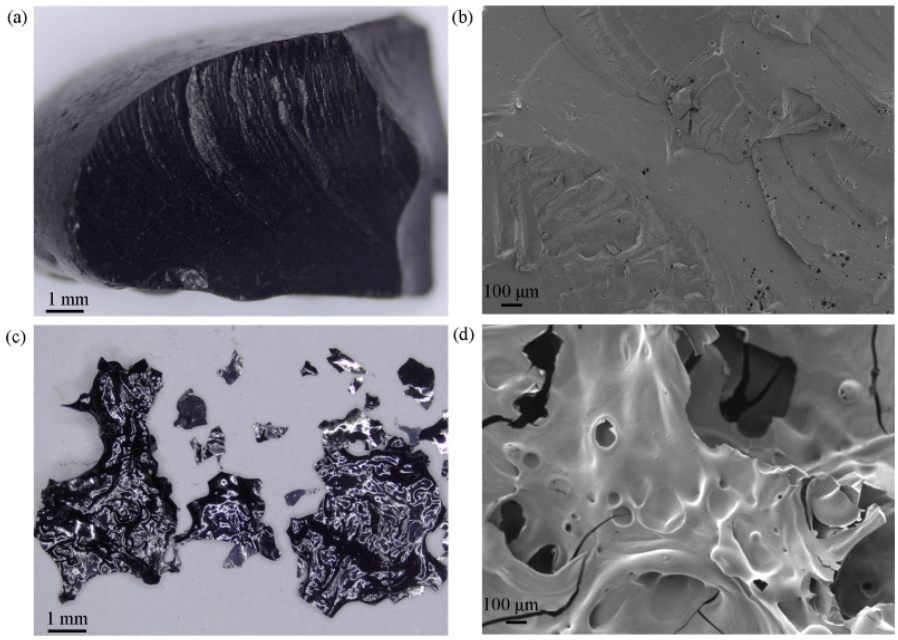

Fig. 13. EM and FESEM images of the asphaltenes before and after pyrolysis. (a) and (c) original sample, (b) and (d) pyrolysis residues.

tensively investigated the impacts of temperature and flow rate on heating rates and kerogen cracking processes (Lai et al., 2017; Kang et al., 2020a), few studies have focused on their effects on product distribution and migration states. As a pyrolytic oil containing both light and heavy components, the boiling point of shale oil is mostly between 180-500 °C (Guo et al., 2024). Moreover, it contains approximately 5%-10%, and in several cases even more than 30% of asphaltene (Kang et al., 2022), which significantly influences reservoir permeability. The asphaltene samples and pyrolysis residues obtained using EM and FESEM are shown in Fig. 13. The original asphaltene exists in a compact solid state (Figs. 13(a) and 13(c)), and the condensed asphaltene contributes to the blockage of pores and fractures in the *in-situ* reservoir. As the temperature increases, asphaltene undergoes secondary cracking and releases gaseous products, resulting in a porous flake residue (Figs. 13(b) and 13(d)). The residue displayed an evident pore structure and experienced significant reductions in mass and volume, and the blocked pores were released after the secondary cracking of asphaltene. Hence, in reservoirs exhibiting noticeable temperature gradients, the injected fluid temperature and flow rate can be optimized to regulate the distribution of oil components within the reservoir, consequently improving reservoir permeability.

Higher fluid temperatures (such as higher than the volatilization temperatures of heavy components) or flow rates can increase the reservoir heating rate and shorten the development period. In this study, these operating conditions were categorized as severe conversion conditions. Under such circumstances, nearly all components of the pyrolysis oil, including asphaltene, vaporize at the pyrolysis front, migrate forward because of the severe thermal or dynamic displacement, and then condense into a mixed state in the low-temperature region, as depicted in Fig. 14(a). The presence of asphaltene in the mixed oil improves its viscosity (Na et al., 2012), and dissolved asphaltene can also precipitate in

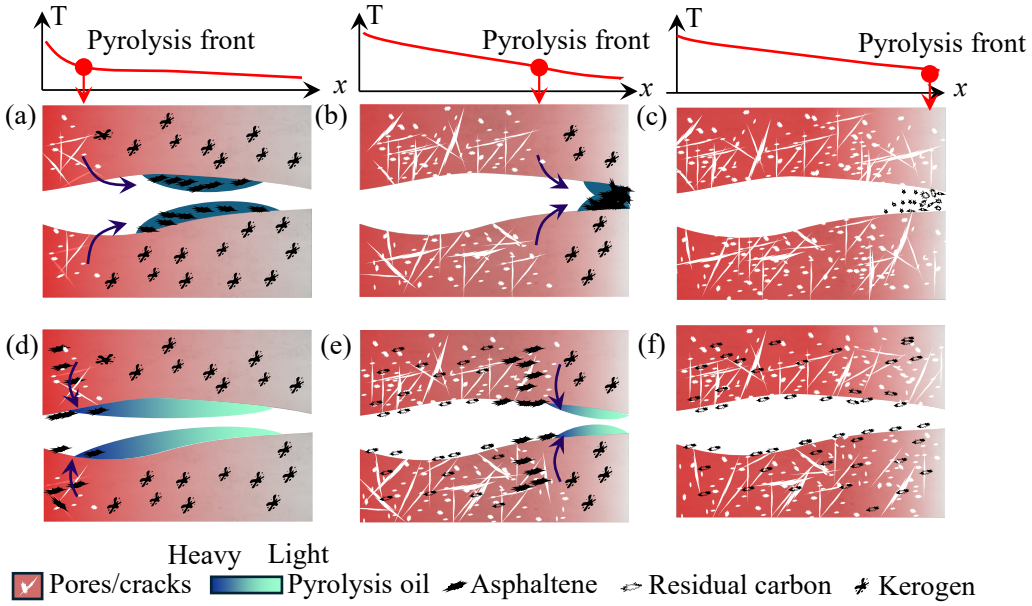

Fig. 14. *In-situ* reservoir state of oil shale under different operating parameters. (a)-(c) represent the evolution of reservoir states under severe conditions and (d)-(f) represent the evolution of reservoir states under mild conditions.

this zone. Both scenarios have the potential to block smaller seepage channels, as shown in Fig. 14(b). As temperature steadily rises in the blocked zone, secondary cracking of asphaltene occurs, resulting in a mass loss exceeding 79%. Subsequently, the released pore space facilitates the elimination of the blockage, as shown in Fig. 14(c). Therefore, reservoir blockage and self-unblocking effects may occur in reservoirs under severe conversion conditions. As a result of reservoir blockage, an increase in the fluid injection pressure and non-uniform pyrolysis occur (Guo et al., 2022), adversely impacting economic returns. Moreover, the production of a large amount of heavy oils and asphaltenes is not conducive to the improvement of oil quality.

Under relatively mild conversion conditions, such as lower heating temperatures (below the boiling points of heavy components) and flow rates, the majority of high-value light oil components with low boiling points tend to volatilize and migrate forward at the pyrolysis front, as shown in Figs. 14(d)-14(e). Simultaneously, heavier components, such as asphaltenes, which possess poor fluidity, remain in the pyrolysis front or within the matrix pores, where secondary cracking occurs *in-situ*, as shown in Figs. 14(e)-14(f). Owing to kerogen cracking, the pores and fractures of the cracked reservoir developed significantly, and blockage by the deposited asphaltene hardly occurred. Consequently, the residual asphaltene did not significantly affect the reservoir permeability in this area. The produced oil primarily comprises light components, thereby preventing reservoir blockage, and the oil quality can be improved under mild conversion conditions.

Thus, the adoption of larger injection fluid parameters is not conducive to the smooth progress and economic feasibility of the *in-situ* conversion process. Reasonable control of the operating parameters, avoiding asphaltene migration, and promoting *in-situ* secondary cracking may be feasible measures to ensure reservoir permeability and improve oil quality.

5. Conclusions

In-situ conversion is recognized as an important method for oil shale production, but the precipitated asphaltene and its thickening effect on the pyrolysis oil damage the reservoir permeability; thus, promoting the *in-situ* pyrolysis of asphaltene is a vital approach to mitigate blockage. In this study, asphaltenes were obtained under different oil shale conversion conditions, and their secondary cracking characteristics were revealed by combining TG and FTIR. The main conclusions are as follows.

1) The mass loss of asphaltenes exceeds 80% at 500 °C, and the obtained asphaltenes under different conversion conditions exhibit significant differences in the cracking process. The maximum mass loss of asphaltene under severe conversion conditions can reach 93.8%. The maximum mass loss of asphaltene produced under mild conversion conditions was ~ 80%. The significant mass loss and volume release provided a direction for eliminating reservoir blockages.
2) The reaction stages were divided based on the activation energies and evolution of the gaseous products. The cracking activation energy of the Asp-N_2 and Asp-*in-situ* samples first remained constant and then gradually increased from 60-200 kJ/mol, whereas that of Asp-water asphaltene was relatively high and showed a trend of first decreasing and then increasing. Based on the evolution of activation energies and pyrolysis gas components, it is believed that asphaltenes obtained under severe conversion conditions undergo a pyrolysis process defined as synchronous two-stage pyrolysis reactions from low-energy bonds to high-energy bonds, whereas asphaltenes obtained under mild conversion conditions undergo a py-

rolysis process defined as sequential three-stage pyrolysis reactions from high-energy bonds to low-energy bonds, and then to high-energy bonds.

3) The behavior of asphaltene in the *in-situ* reservoir under different conditions, and a suggestion for eliminating reservoir blockage was proposed based on secondary cracking characteristics. Higher conversion parameters can cause asphaltene migration and deposition, leading to reservoir blockage. Reasonable control of operating parameters, inhibition of asphaltene migration, and promotion of *in-situ* secondary cracking may be feasible measures to ensure reservoir permeability and enhance oil quality.

Acknowledgements

This work was supported by the National Natural Science Fund Project of China (No. 42302350), the National Key R&D Program of China (Nos. 2019YFA0705502 and 2019YFA0705501), and the Young and Middle-aged Excellent Team Project for Scientific and Technological Innovation of Jilin Province, China (No. 20220508135RC).

Conflict of interest

The authors declare no competing interest.

References

Aboyade, A. O., Carrier, M., Meyer, E. L., et al. Model fitting kinetic analysis and characterisation of the devolatilization of coal blends with corn and sugarcane residues. Thermochimica Acta, 2012, 530: 95-106.

Akmaz, S., Gurkaynak, M. A., Yasar, M. The effect of temperature on the molecular structure of Raman asphaltenes during pyrolysis. Journal of Analytical and Applied Pyrolysis, 2012, 96: 139-145.

Allix, P., Burnham, A., Fowler, T., et al. Coaxing oil from shale. Oilfield Review, 2010, 22(4): 4-15.

Brandt, A. R. Converting oil shale to liquid fuels: Energy inputs and greenhouse gas emissions of the Shell *in situ* conversion process. Environmental Science & Technology, 2008, 42(19): 7489-7495.

Braun, R. L., Burnham, A. K. Mathematical model of oil generation, degradation, and expulsion. Energy & Fuels, 1990, 4(2): 132-146.

Braun, R. L., Rothman, A. J. Oil-shale pyrolysis: Kinetics and mechanism of oil production. Fuel, 1975, 54(2): 129-131.

Douda, J., Alvarez, R., Bolaños, J. N. Characterization of Maya asphaltene and maltene by means of pyrolysis application. Energy & Fuels, 2008, 22(4): 2619-2628.

Fei, Y., Marshall, M., Jackson, W. R., et al. Evaluation of several methods of extraction of oil from a Jordanian oil shale. Fuel, 2012, 92(1): 281-287.

Gregorčič, G., Lightbody, G. Gaussian process approach for modelling of nonlinear systems. Engineering Applications of Artificial Intelligence, 2009, 22(4-5): 522-533.

Gu, J., Deng, S., Sun, Y., et al. Pyrolysis behavior and pyrolysate characteristics of Huadian oil shale kerogen catalyzed by nickel-modified montmorillonite. Advances in Geo-Energy Research, 2024, 11(3): 168-180.

Guo, W., Fan, C., Liu, Z., et al. Fates of pyrolysis oil components in the non-isothermal propped fractures during oil shale *in situ* pyrolysis exploitation. Energy, 2024, 288: 129851.

Guo, W., Shui, H., Liu, Z., et al. Reliability analysis of elastic graphite packer in heat injection well during oil shale *in-situ* conversion. Advances in Geo-Energy Research, 2023, 7(1): 28-38.

Guo, W., Yang, Q., Deng, S., et al. Experimental study of the autothermic pyrolysis *in-situ* conversion process (ATS) for oil shale recovery. Energy, 2022, 258: 124878.

Han, X., Kulaots, I., Jiang, X., et al. Review of oil shale semicoke and its combustion utilization. Fuel, 2014, 126: 143-161.

Hao, J., Che, Y., Tian, Y., et al. Thermal cracking characteristics and kinetics of oil sand bitumen and its SARA fractions by TG-FTIR. Energy & Fuels, 2017, 31(2): 1295-1309.

He, W., Sun, Y., Guo, W., et al. Controlling the *in-situ* conversion process of oil shale via geochemical methods: A case study on the Fuyu oil shale, China. Fuel Processing Technology, 2021, 219: 106876.

Hu, S., Wu, H., Liang, X., et al. A preliminary study on the eco-environmental geological issue of *in-situ* oil shale mining by a physical model. Chemosphere, 2022, 287: 131987.

Kang, S., Sun, Y., Qiao, M., et al. The enhancement on oil shale extraction of $FeCl_3$ catalyst in subcritical water. Energy, 2022, 238: 121763.

Kang, Z., Zhao, Y., Yang, D. Review of oil shale *in-situ* conversion technology. Applied Energy, 2020a, 269: 115121.

Kang, Z., Zhao, Y., Yang, D., et al. A pilot investigation of pyrolysis from oil and gas extraction from oil shale by *in-situ* superheated steam injection. Journal Petroleum Science Engineering, 2020b, 186: 106785.

Khakimova, L., Bondarenko, T., Cheremisin, A., et al. High pressure air injection kinetic model for Bazhenov Shale Formation based on a set of oxidation studies. Journal of Petroleum Science and Engineering, 2019, 172: 1120-1132.

Khulbe, K. C., Sachdev, A. K., Mann, R. S., et al. TGA studies of asphaltenes derived from Cold-Lake (Canada) bitumen. Fuel Processing Technology, 1984, 8(3): 259-266.

Kumar, R., Bansal, V., Badhe, R. M., et al. Characterization of Indian origin oil shale using advanced analytical techniques. Fuel, 2013, 113: 610-616.

Lai, D., Zhan, J., Tian, Y., et al. Mechanism of kerogen pyrolysis in terms of chemical structure transformation. Fuel, 2017, 199: 504-511.

Li, R., Jin, B., Zhong, Z., et al. Research on biomass pyrolysis three-pseudocomponent model by Gaussian multi-peaks fitting. Acta Energiae Solaris Sinica, 2010, 31(7): 806-

810.

Liu, Y., Yao, Q., Sun, M., et al. Selective preparation of light aromatic hydrocarbons from catalytic fast pyrolysis vapors of coal tar asphaltene over transition metal ion modified zeolites. Chinese Journal of Chemical Engineering, 2021, 35: 275-287.

Liu, Z., Sun, Y., Guo, W., et al. Reservoir-scale study of oil shale hydration swelling and thermal expansion after hydraulic fracturing. Journal of Petroleum Science and Engineering, 2020, 195: 107619.

Luo, C., Liu, H., Zhou, S., et al. Catalytic role of various clay minerals during the thermal reaction process with oxidized and pyrolyzed oils. Journal of Thermal Analysis and Calorimetry, 2024: 149: 8681-8691.

Martins, M. F., Salvador, S., Thovert, J. F., et al. Co-current combustion of oil shale-Part 2: Structure of the combustion front. Fuel, 2010, 89(1): 133-143.

Ma, S., Li, S., Zhang, Z., et al. The feasibility study of *in situ* conversion of oil shale based on calcium-oxide-based composite materia hydration exothermic reaction. Energies, 2024, 17(8): 1798.

Ma, W., Wang, S., Cui, J., et al. Thermal decomposition kinetic model of phenolic resin. Acta Physico-Chimica Sinica, 2008, 24(6): 1090-1094.

Metz, W. D. Oil shale: A huge resource of low-grade fuel. Science, 1974, 184(4143): 1271-1275.

Murugan, P., Mahinpey, N., Mani, T. Thermal cracking and combustion kinetics of asphaltenes derived from Fosterton oil. Fuel Processing Technology, 2009, 90(10): 1286-1291.

Na, J. G., Im, C. H., Chung, S. H., et al. Effect of oil shale retorting temperature on shale oil yield and properties. Fuel, 2012, 95: 131-135.

Nguimbi, G. R., Sun, Y., Guo, M., et al. Thermogravimetric and kinetic analysis on pyrolysis and combustion of oil shale under different oxygen concentration atmosphere. International Journal of Earth Sciences and Engineering, 2016, 9(1): 66-73.

Pan, Y., Zheng, L., Liu, Y., et al. A review of the current status of research on convection-heated *in-situ* extraction of unconventional oil and gas resources (oil shale). Journal of Analytical and Applied Pyrolysis, 2023, 175: 106200.

Pei, S., Huang, L., Zhang, L., et al. Experimental study on thermal cracking reactions of ultra-heavy oils during air injection assisted *in-situ* upgrading process. Journal of Petroleum Science and Engineering, 2020, 195: 107850.

Pei, S., Wang, Y., Zhang, L., et al. An innovative nitrogen injection assisted in-situ conversion process for oil shale recovery: Mechanism and reservoir simulation study. Journal of Petroleum Science and Engineering, 2018, 171: 507-515.

Qian, J., Wang, J., Li, S. Oil shale development in China. Oil Shale, 2003, 20(3): 356-359.

Qing, W., Wang, X., Shuo, P. Study on the structure, pyrolysis kinetics, gas release, reaction mechanism, and pathways of Fushun oil shale and kerogen in China. Fuel Processing Technology, 2022, 225: 107058.

Rüger, C. P., Neumann, A., Kösling, P., et al. Addressing thermal behavior and molecular architecture of asphaltenes by a thermal-optical carbon analyzer coupled to high-resolution mass spectrometry. Energy & Fuels, 2022, 36(17): 10177-10190.

Saitova, A., Strokin, S., Ancheyta, J. Evaluation and comparison of thermodynamic and kinetic parameters for oxidation and pyrolysis of Yarega heavy crude oil asphaltenes. Fuel, 2021, 297: 120703.

Shi, J., Ma, Y., Li, S., et al. Characteristics of Estonian oil shale kerogen and its pyrolysates with thermal bitumen as a pyrolytic intermediate. Energy & Fuels, 2017, 31(5): 4808-4816.

Sun, Y., Liu, Z., Li, Q., et al. Controlling groundwater infiltration by gas flooding for oil shale *in situ* pyrolysis exploitation. Journal of Petroleum Science and Engineering, 2019, 179: 444-454.

Tirado, A., Félix, G., Al-Muntaser, A. A., et al. Molecular asphaltene transformations during aquathermolysis of heavy crude oil: analysis of the literature data. Energy & Fuels, 2023, 37(11): 7927-7944.

Vyazovkin, S., Burnham, A. K., Criado, J. M., et al. ICTAC Kinetics Committee recommendations for performing kinetic computations on thermal analysis data. Thermochimica Acta, 2011, 520(1-2): 1-19.

Wang, L., Zhao, Y., Yang, D., et al. Effect of pyrolysis on oil shale using superheated steam: A case study on the Fushun oil shale, China. Fuel, 2019, 253: 1490-1498.

Wang, Q., Wang, X., Liu, H., et al. Study of the combustion mechanism of oil shale semi-coke with rice straw based on Gaussian multi-peak fitting and peak-to-peak methods. Oil Shale, 2013, 30(2): 157-172.

Wu, T., Xue, Q., Li, X., et al. Extraction of kerogen from oil shale with supercritical carbon dioxide: Molecular dynamics simulations. The Journal of Supercritical Fluids, 2016, 107: 499-506.

Xu, S., Sun, Y., Lü, X., et al. Effects of composition and pore evolution on thermophysical properties of Huadian oil shale in retorting and oxidizing pyrolysis. Fuel, 2021, 305: 121565.

Yang, Q., Zhang, X., Xu, S., et al. Low-temperature co-current oxidizing pyrolysis of oil shale: Study on the physicochemical properties, reactivity and exothermic characters of semi-coke as heat generation donor. Journal of Petroleum Science and Engineering, 2022, 216: 110726.

Yan, J., Jiang, X., Han, X. Study on the characteristics of the oil shale and shale char mixture pyrolysis. Energy & Fuels, 2009, 23(12): 5792-5797.

Zhu, C., Guo, W., Sun, Y., et al. Reaction mechanism and reservoir simulation study of the high-temperature nitrogen injection *in-situ* oil shale process: A case study in Songliao Basin, China. Fuel, 2022, 316: 123164.